Solubilization of carbon nanotubes with ethylene-vinyl acetate for solution-processed conductive films and charge extraction layers in perovskite solar cells

Giulio Mazzotta[1], Markus Dollmann[1], Severin N. Habisreutinger[1†], M. Greyson Christoforo[1], Zhiping Wang[1], Henry J. Snaith[1], Moritz K. Riede[1] and Robin J. Nicholas[1]*

[1] University of Oxford, Department of Physics, Clarendon Laboratory, Parks Road, Oxford, OX1 3PU, United Kingdom.

ABSTRACT Carbon nanotube (CNT) solubilization via non-covalent wrapping of conjugated semiconducting polymers is a common technique used to produce stable dispersions for depositing CNTs from solution. Here, we report the use of a non-conjugated insulating polymer, ethylene-vinyl acetate (EVA), to disperse multi- and single-walled CNTs (MWCNT and SWCNT) in organic solvents. We demonstrate that despite the insulating nature of the EVA, we can produce semi-transparent films with conductivities of up to 34 S/cm. We show, using photoluminescence spectroscopy, that the EVA strongly binds to individual CNTs thus making them soluble, preventing aggregation, and facilitating the deposition of high quality films. To prove the good electronic properties of this composite, we have fabricated perovskite solar cells using

EVA/SWCNT and EVA/MWCNTs as selective hole contact, obtaining power conversion efficiencies of up to 17.1%, demonstrating that the insulating polymer does not prevent the charge transfer from the active material to the CNTs.

KEYWORDS: Carbon nanotubes, conductive films, CNT polymer functionalization, insulating polymer, perovskite solar cells.

INTRODUCTION

In recent years carbon nanotubes have attracted a lot of interest due to their unique electronic, mechanical, thermal and optical properties, making them a promising candidate for conductive coatings, electronic sensors, energy conversion and storage applications.[1]

Their widespread application, however, is hindered by difficulties processing them due to their high aspect ratio and strong van der Waals interactions,[2] making dispersions unstable due to the quick aggregation of the nanotubes. Non-covalent complexation is a widely used strategy to purify and solubilize nanotubes without altering their electronic structure and the use of conjugated polymers in this process[3] has been proven to be an effective way to produce electronic grade films used in transistors,[4,5] sensors[6] and solar cells.[7,8]

In this purification process,[9,10] CNTs are added to a polymer solution and treated with an ultrasonic probe to break up CNT bundles and allow the polymer to bind to individual tubes. The mixture is then centrifuged to remove non-functionalized particles and impurities. The supernatant, containing the functionalized nanotubes, is diluted with a less polar solvent to induce the aggregation of the nanotubes and separate them from the excess polymer, which remains dissolved.

Finally, the solution is centrifuged once more and the precipitate, containing the polymer-CNT nanohybrids, is dispersed in an organic solvent such as chlorobenzene, chloroform or toluene. This method typically involves the use of expensive conjugated polymers since the π-π stacking interaction is thought to be one of the main driving mechanisms by which polymers can interact and bind with the CNTs to make them dispersible.[11]

The solubilization with polymers can have several benefits over solubilizing CNTs using other surfactants such as chelating salts, which require an aqueous environment. This includes the easy removal of excess polymer, quick extraction of the wrapped CNT species and the use of organic solvents, making the process suitable to applications which are not water compatible.

In this paper, we show how an inexpensive non-conjugated, insulating polymer, ethylene-vinyl acetate (EVA, structural formula in the inset of **Figure 1**), can solubilize both single- and multi-walled CNTs in organic solvents to produce a uniform and stable dispersion, and by removing the excess polymer, it can be deposited to form semi-transparent conductive films.

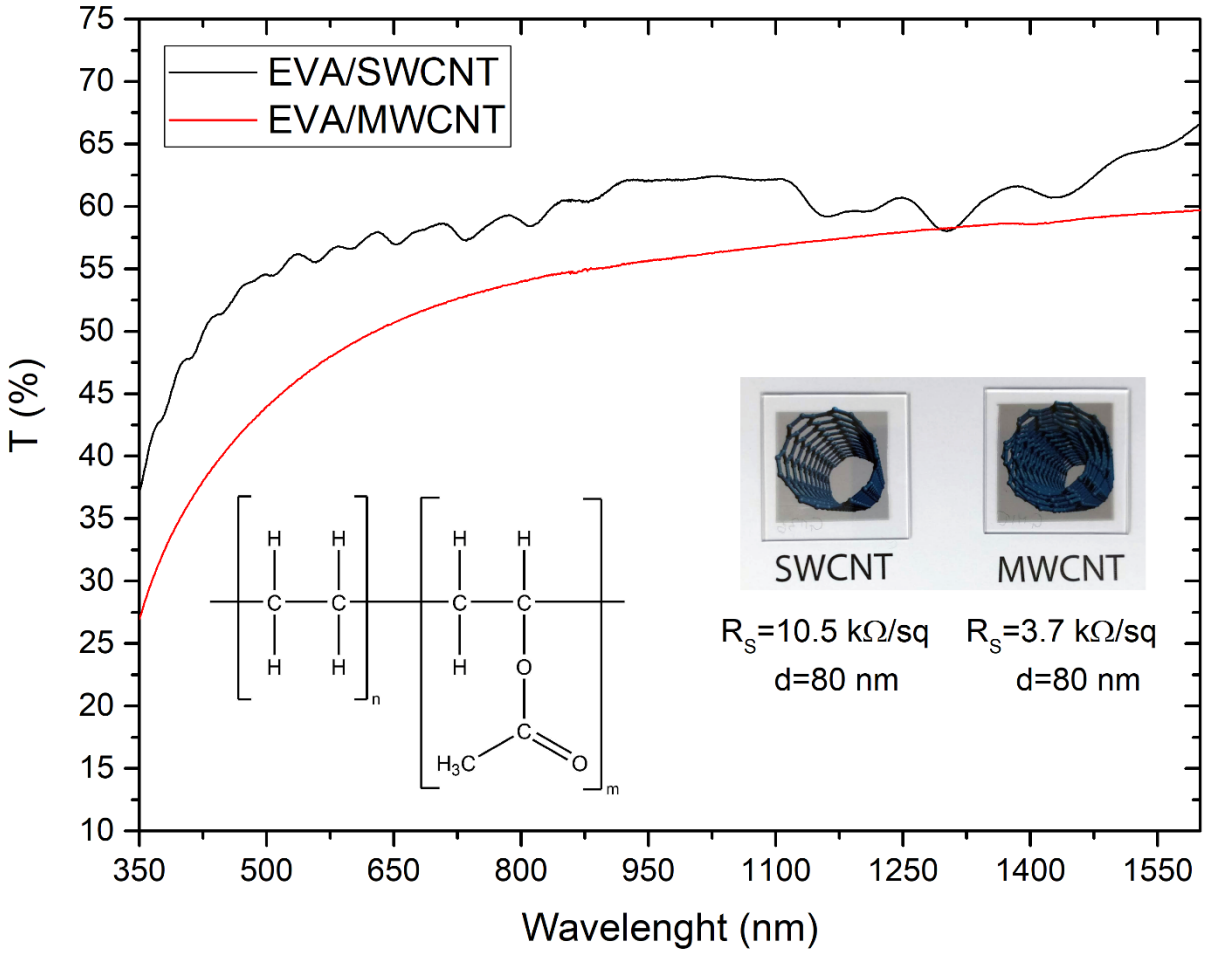

Figure 1. Transmittance spectrum of the sprayed EVA/SWCNT and EVA/MWCNT films on glass. The left inset shows the structural formula of EVA. The right inset shows an image of the semi-transparent films, having a 47% transmittance at 550 nm for MWCNT and 56% for SWCNT tubes. The losses due to the glass substrate have not been removed. The films have both a thickness of 80 nm and an electrical conductivity of 10.5 kΩ/sq and 3.7 kΩ/sq respectively, corresponding to a conductivity of 12 S/cm and 34 S/cm.

EVA is a widely used polymer in the manufacture of products where good mechanical and hydrophobic properties are required, such as food packaging, flexible hoses, footwear components

or car bumpers. Due to its low cost and low water vapor transmission rate (WVTR)[12] it is currently the standard encapsulation material for silicon solar cell modules.

With the conjugated-polymer accounting for up to 50% of the materials cost in the wrapping of single-walled carbon nanotubes, replacing it with EVA, which can be three orders of magnitude cheaper, the cost of the process is reduced to little more than the cost of the nanotubes alone. In an even more significant finding we demonstrate that the use of EVA allows us to replace the SWCNTs with MWCNTs, for which there are fewer solubilization processes reported in literature, and yet remove the excess polymer to fabricate conductive films, which can reduce the overall cost by a further substantial factor. (e.g. from ~900 €/m^2 for P3HT/SWCNT to ~80 €/m^2 for MWCNT/EVA with our lab-scale process described in this paper, with the realistic potential of a further ten-fold reduction on a large scale production).[13]

EVA/CNT composites obtained by solution mixing have been investigated to fabricate conductive films for different applications. Zhang et al.[14] demonstrated the use of an EVA/CNT composite with a conductivity of 2.5×10^{-2} S/cm as a supercapacitor electrode for flexible energy-storage, while Das et al.[15] showed the use of films with a conductivity of 1×10^{-4} S/cm for electromagnetic interference (EMI) shielding applications.

RESULTS AND DISCUSSION

We prepared EVA/CNT dispersions in chloroform using a solubilization process, where we used EVA instead of the commonly employed conjugated polymers (details described in **Methods**). To study the electrical and optical properties of the composite, the resulting solutions have been deposited as thin films on glass substrates by spray coating. **Figure 1** shows the transmittance spectra and an image of the resulting films. The black solid line shows the absorbance of the SWCNT film on glass (reflection losses due to the glass substrate, ~4%, have not been removed).

This film has a transparency between 55 % and 75% in the near infrared region, dropping to values of 40-55% in the visible region due to the E_{22} and M_{11} transitions of the nanotubes, which are visible as individual excitonic absorption features from the different nanotube species present in the starting material[16]. The sprayed film has a thickness of 80 nm and a sheet resistance of 10.5 kΩ/sq, corresponding to a conductivity of 12 S/cm. The conductivity of this film is three orders of magnitude higher than previously reported composites of EVA and carbon nanotubes.[14]

The red solid line shows the transmittance spectrum of a MWCNT/EVA film which shows a continuous absorption of the MWCNT, which, due to the presence of multiple shells of several diameters in each tube, does not show Van Hove singularity peaks. The 80 nm thick film has a sheet resistance of 3.7 kΩ/sq, corresponding to a conductivity of 34 S/cm. We want to emphasize that this is the first time that such polymer purification process is used with MWCNTs, as previously reported solubilizations do not involve the removal of the excess polymer.[17] We speculate that this step leads to a much enhanced inter-tube contact and better connected percolation paths, which in turn results in a conductivity increase by several order of magnitudes.

To get a better understanding of the properties of the CNT/EVA dispersion in solvents, we measured the photoluminescence excitation (PLE) map, shown in **Figure 2**. This was done for SWCNTs only, as due to the presence of multiple shells in MWCNTs any photogenerated carriers can relax non-radiatively through the outer shells, so all the photoluminescence is quenched. The emission spectrum corresponds to the E_{11} emission following excitation to the state E_{22} of 10 different chiralities [(7,5), (7,6), (8,4), (8,6), (8,7), (9,4), (9,5), (9,7), (10,3), (10,5)] SWCNT. This process is shown schematically in the inset diagram of **Figure 2**.

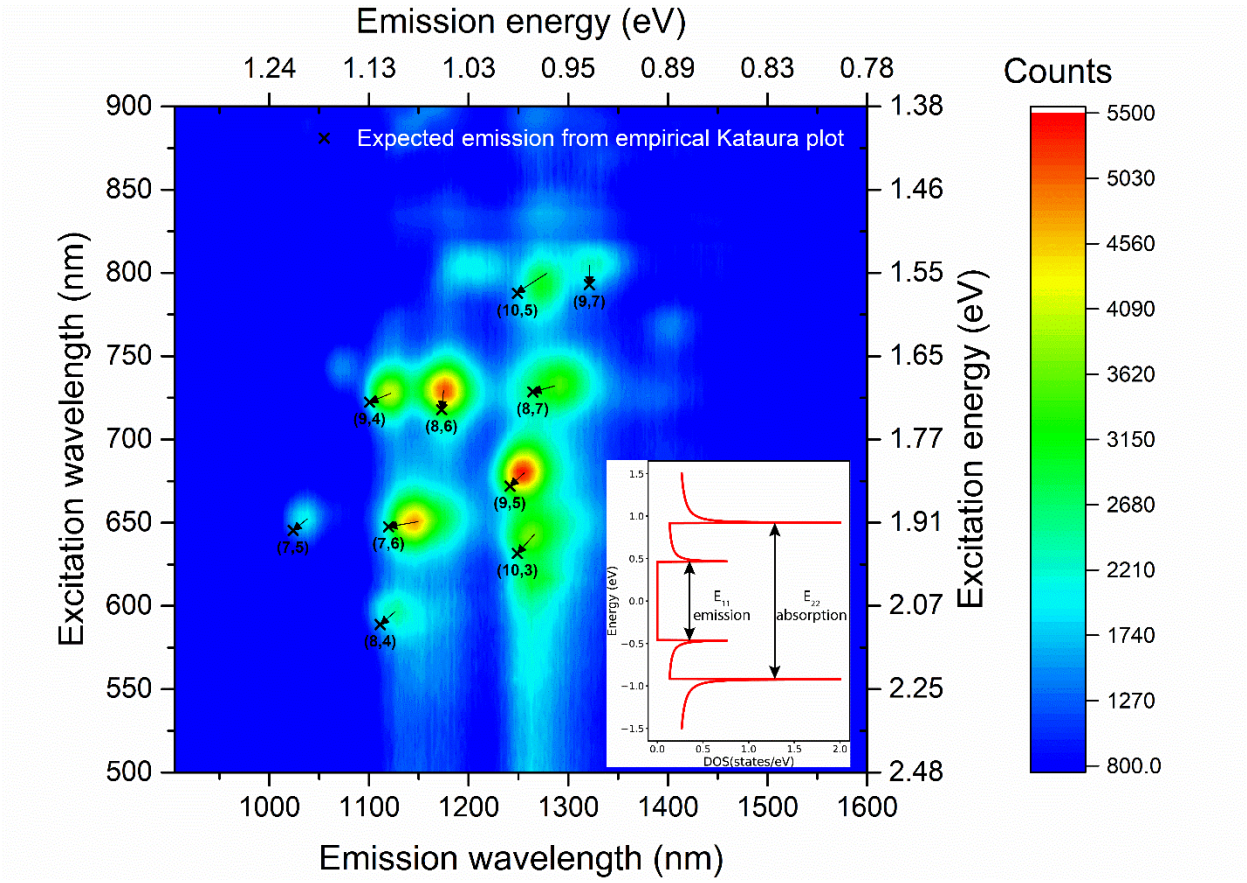

Figure 2. Photoluminescence excitation (PLE) maps of EVA/SWCNT composites. Carbon nanotubes are excited at the Van Hove singularity associated with the E_{22} transition and emit from the E_{11}, as shown in the inset diagram representing the typical density of states of a semiconducting carbon nanotube (excitonic effects neglected for illustrative purposes). Individually resolved peaks show well-dispersed nanotubes and scarcity of bundles, which would quench the photoluminescence. The black crosses mark the expected emissions of SWCNT dispersed in water from a semi-empirical model[18], and the arrows show the shift from the observed peak, caused by the different dielectric environment due to the solvent and to the mechanical stress on the CNT.

The numerous peaks observed indicate a non-selective solubilization, which enables a much higher concentration of solubilized tubes compared to selective polymers. The presence of individually resolved peaks suggests the ability of EVA to prevent the formation of SWCNT bundles, which would quench the photoluminescence from individual tubes due to charge transfer and reabsorption by other SWCNT species and quenching by metallic tubes.[19,20] The black crosses mark the expected emission as predicted from a semi-empirical model by Weisman at al.[18] for tubes dispersed using an aqueous surfactant. As the optical properties of the nanotubes depend solely on the chiral indices of the tube, the model can be used as a reference.

The observed redshift is caused by two different factors: first, by a changed dielectric environment due to the different solvent and surfactant which can cause screening of the excitonic Coulomb interactions,[21] and second by mechanical strain in the tubes caused by a strong polymer-nanotube interaction,[22] which can result in small energy shifts for the tubes depending on their chiral indices.

Semiconducting SWCNTs can be classified using the graphene wrapping condition $m - n = 3p + q$, where m and n are the chiral indexes, p is any integer and the value $q=\pm1$ for semiconducting tubes is used as a classification parameter. As shown by Yang and Han,[23] SWCNTs show a different behavior under mechanical strain depending on the q value, resulting in an increased E_{11} transition energy for $q=+1$ and a decrease for $q=-1$, and the opposite for the E_{22} transition. As shown elsewhere,[22] to further analyze the mechanical strain induced by the polymer we can separate the energy shift into two different contributions

$$\Delta E_{ii}=\Delta E_{environment}+\Delta E_{strain} \quad (1)$$

where the $\Delta E_{environment}$ is the contribution from the different environment due to the different solvent used compared to the semi-empirical model. This leads to a shift of similar magnitude and

sign in the emission and in the absorption, irrespective of the tube chirality. The second component of Equation (1), ΔE_{strain}, is given by the mechanical strain on the tube, which depends on the tube chirality and has the same trend for the same q values. Having a similar magnitude for the E_{11} or E_{22} transition, $\Delta E_{environment}$ is taken as the mean red shift $(\Delta E_{11}+\Delta E_{22})/2$ and ΔE_{strain} will be the semi-difference $\Delta E_{strain}=(\Delta E_{11} - \Delta E_{22})/2$.

ΔE_{strain} can be predicted as shown previously[22–24] using the expression

$$\Delta E_{strain}=\frac{\Delta E_{11} - \Delta E_{22}}{2}=\left(\frac{2\, t_0 a_{c\text{-}c}}{d}\right)(\varepsilon_{\perp} - \nu\varepsilon_{\parallel})+3qt_0[(1+\nu)\varepsilon_{\parallel}\cos(3\theta)+\varepsilon_{\perp}\sin(3\theta)] \qquad (2)$$

where t_0 = 3.0 eV is the carbon-carbon transfer integral, $a_{c\text{-}c}$ = 1.432 Å is the bond length, d is the diameter of the nanotube, θ is the chiral angle of the nanotube, ν = 0.2 is Young's modulus, and $\varepsilon_{\perp}$ and $\varepsilon_{\parallel}$ are the perpendicular and longitudinal strains.

Figure 3 shows the energy shifts due to mechanical strain which have been multiplied by the q values to give the same trend for both species for ease of visualization. The solid line in **Figure 3** shows the fit to Equation (1) yielding values of longitudinal strain $\varepsilon_{\parallel}$ = –0.23 % and perpendicular strain $\varepsilon_{\perp}$ = 0.14 %. Despite the relatively large errors, the data clearly show a trend predicted well by the model, indicating a significant strain on the tubes that we attribute to a strong binding of the polymer to the tube.

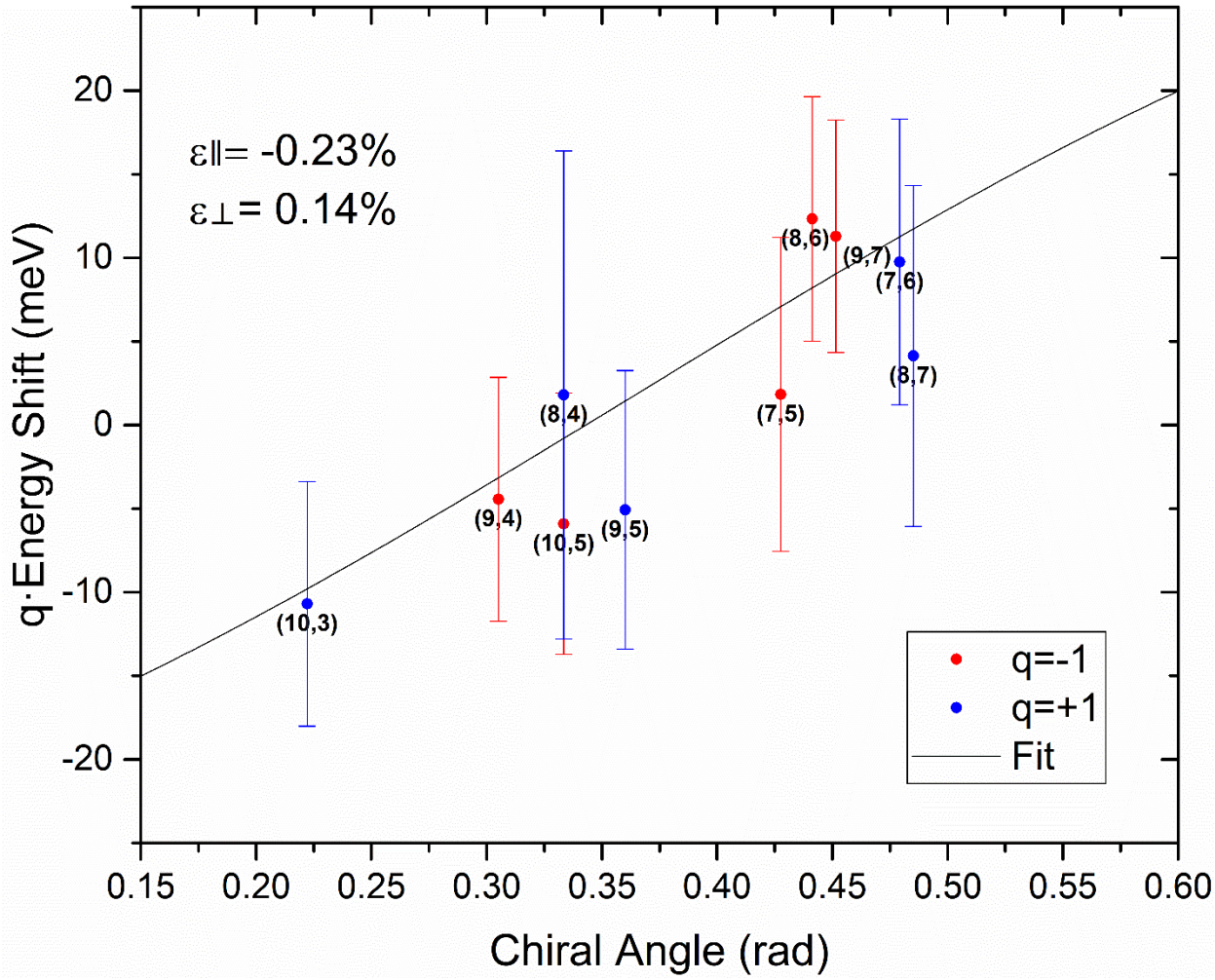

Figure 3. Energy shift caused by mechanical strain on the tube as a function of the chiral angle θ. Values have been multiplied by the parameter q to better show the trend given by the model of equation (2). The solid line shows the expected energy shift for tubes with longitudinal strain $\varepsilon_{\parallel}$ = −0.23 % and perpendicular strain $\varepsilon_{\perp}$ = 0.14 %.

The absence of π orbitals in the EVA polymer excludes the wrapping mechanism shown by polymers commonly used in organic electronics. The presence of numerous CH-groups, however, could explain the strong binding inferred from the PL shift, as CH-π interactions have been shown

to be the driving mechanism for binding between non-conjugated polymers and nanotubes,[17] although purifications routes to remove the unbound polymer and the electrical properties of the nanohybrids have never been studied on these systems. Despite being much weaker than the π-π interaction, the high number of -CH groups in the EVA polymer could provide sufficient binding force. Furthermore, the low glass transition of the polymer (T_G= –43°C)[25] is indicative of a low rigidity of the polymer backbone, allowing it to easily wrap along the side wall of the nanotubes permitting numerous interactions with the -CH groups.[26]

To study the morphology of individual tubes, a diluted EVA/CNT solution was deposited on glass by spin-coating. **Figure 4a** and **4c** show an AFM image of the resulting sample for SWCNTs and MWCNTs, respectively, with the height profiles shown in **Figure 4b** and **4d**. The profile lines show numerous regions on the SWCNT with a height of 1 to 2 nm, suggesting a thin polymer coating of one or two layers around a single nanotube.[27] Other regions show a thicker profile of up to 10-11 nm (Profile 2), probably due to some bundled tubes or a thicker polymer coating, the latter suggests that the polymer-wrapping is a non-self-limiting process. The MWCNT samples show again a very thin height profile (5-7 nm in the thinnest regions, up to 25 nm in the thickest), also suggesting single or small bundle solubilization. It is worth noting that despite the AFM studies showing the possibility of nanotube bundles in the films, the very well-defined peaks in the PLE map (**Figure 2**) suggest a very limited bundling of tubes in the SWCNT dispersion, since bigger bundles of tubes would broaden and quench the PL emission due to the large number of metallic nanotubes in the dispersion (shown by Raman measurements in Figure S2).

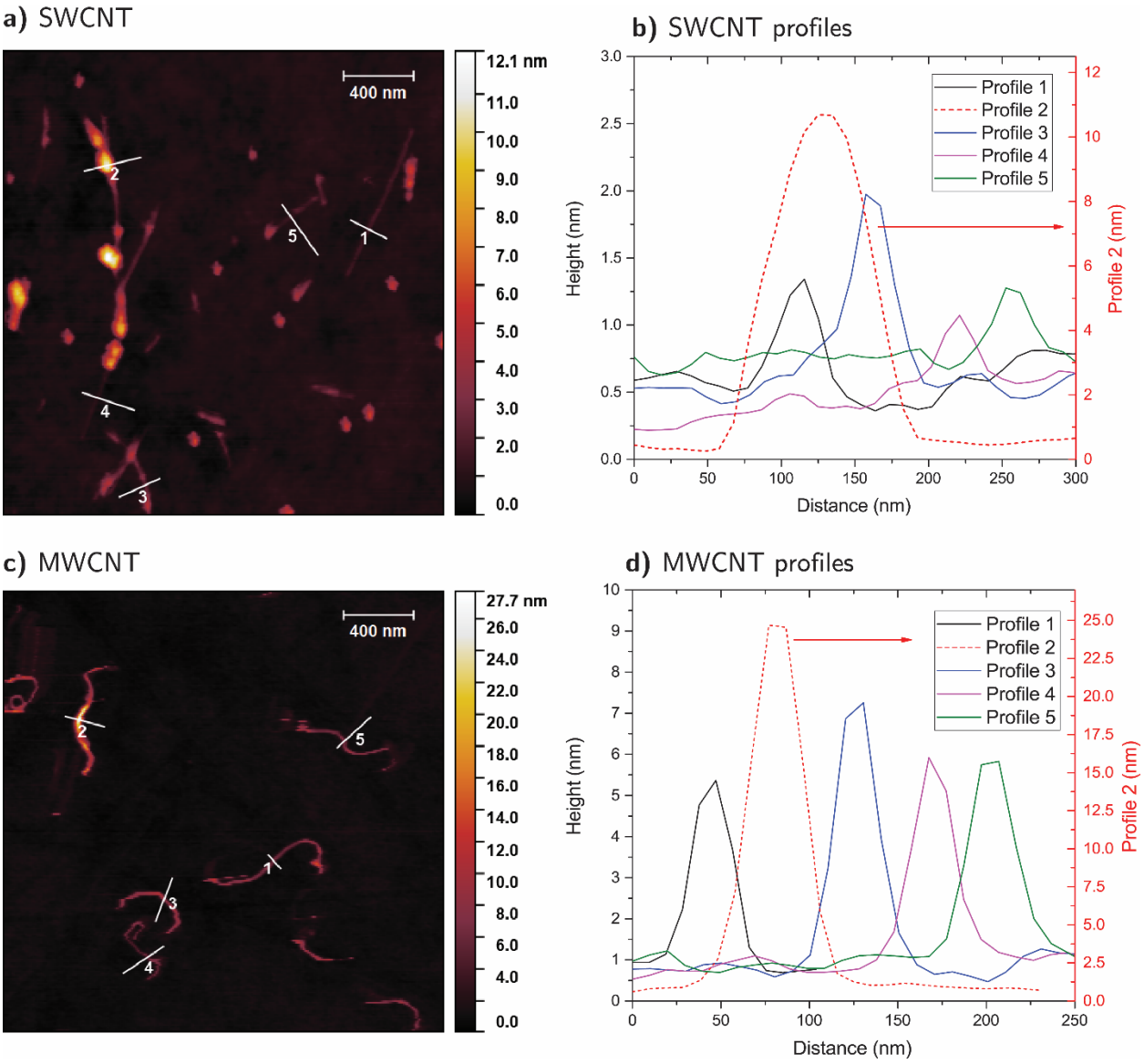

Figure 4. AFM image of diluted EVA/SWCNT **(a)** and EVA/MWCNT **(c)** nanohybrids on glass, and height profiles along the white segments on the AFM maps for EVA/SWCNT **(b)** and EVA/MWCNT **(d).** Profile 2 is plotted on a different scale (right Y axes) in both graphs.

To demonstrate the excellent electronic properties of the EVA/CNT system in a device application, we used these nanohybrids as highly conductive charge extraction channels in two different perovskite solar cells. SWCNTs wrapped with a semiconducting polymer such as poly(3-hexylthiophene) (P3HT) have been successfully employed as hole transporting layer in perovskite solar cells,[28] demonstrating that the CNTs remove the need for lithium based dopants in the hole transporting layer based on 2,2',7,7'-Tetrakis[N,N-di(4-methoxyphenyl)amino]-9,9'-spirobifluorene (Spiro-OMeTAD). We have fabricated analogous devices where we replace the P3HT/SWCNTs with EVA/CNTs. The device stack is shown in **Figure 5**. The electron-collecting transparent electrode is made of fluorine-doped tin oxide (FTO), on which a planar layer of tin oxide (SnO_2) is deposited. SnO_2 act as a charge-selective layer accepting photogenerated electrons from the perovskite whiles simultaneously blocking holes.

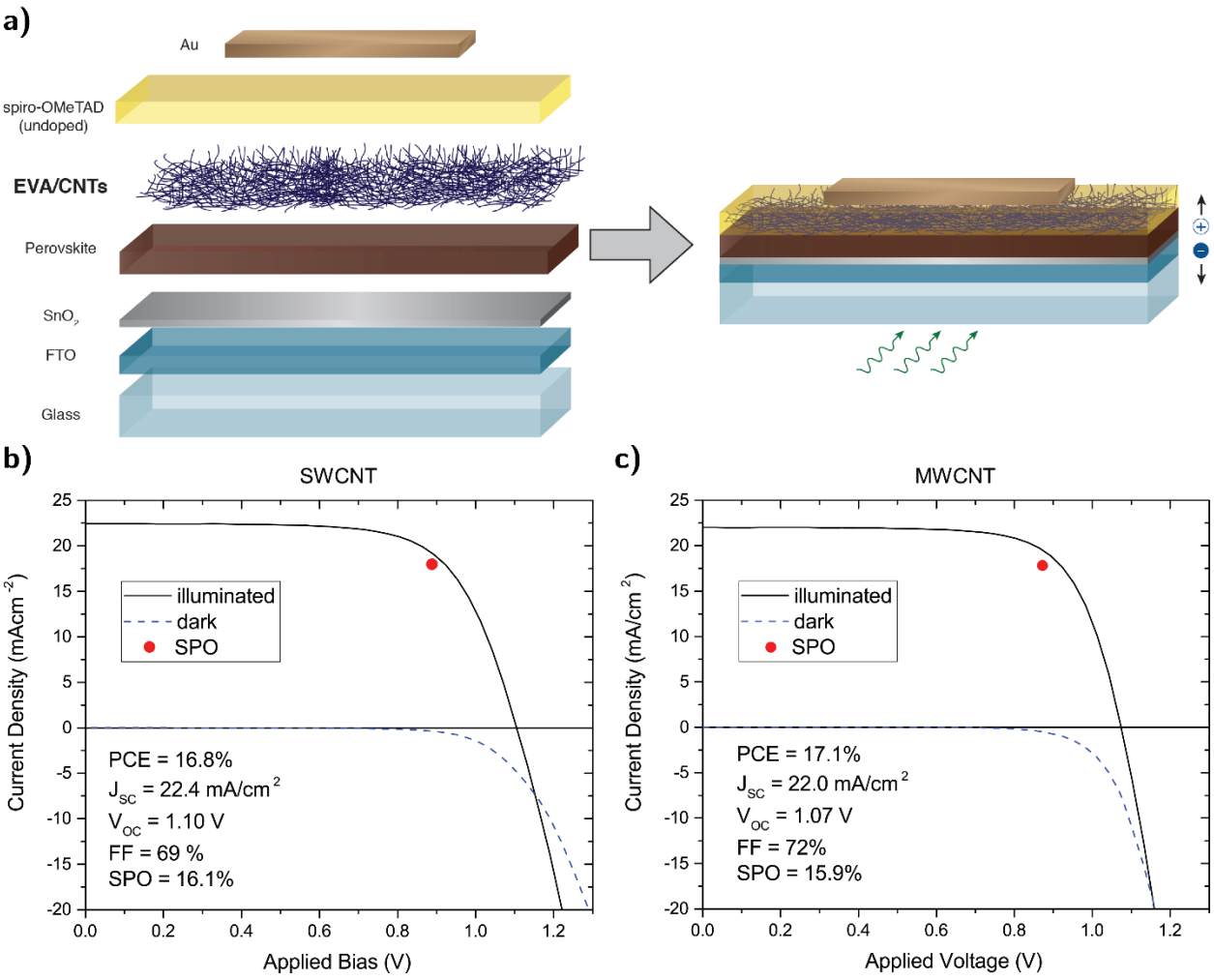

Figure 5. a) Schematic representation of the solar cell. A transparent electrode (FTO) collects electrons from the n-type SnO_2 layer, on top of which a perovskite ($FA_{0.83}MA_{0.17}Pb(I_{0.83}Br_{0.17})_3$ for SWCNT devices and $FA_{0.83}Cs_{0.17}Pb(I_{0.9}Br_{0.1})_3$ for MWCNT devices) absorbs light and generates charges. The p-type layer is a network of EVA/CNTs infiltrated with undoped spiro-OMeTAD, and the hole-collecting electrode is a gold film. **Bottom**: JV curves of devices using EVA/MWCNT **(b)** and EVA/SWCNT **(c)** as hole transporting layers. The black curve represents the scan under illumination (1 sun), while the blue dashed curve is obtained in the dark, the red dot is the steady-state point of maximum power output.

To show the versatility of the technology, we demonstrate the architecture with two different mixed perovskites absorbers, $FA_{0.83}MA_{0.17}Pb(I_{0.83}Br_{0.17})_3$ with SWCNTs and $FA_{0.83}Cs_{0.17}Pb(I_{0.9}Br_{0.1})_3$ with the MWCNTs, both of which are known to produce high performance perovskite solar cells.[29–32] The hole transporting layer is a spray-coated film of EVA/CNT, on which a layer of un-doped spiro-OMeTAD is then deposited by spin-coating in order to infiltrate the EVA/CNT film and preventing a direct contact of the perovskite with the top gold electrode.

The JV curves of the best devices are shown in **Figure 5**. The power conversion efficiency (PCE) was 16.8% for devices with EVA/SWCNT and 17.1% for EVA/MWCNT, with a steady-state power output (SPO), obtained by holding the cell at the maximum power point voltage (V_{MPP}) for extended time, of 15.9% and 16.1% respectively. EVA/SWCNT devices showed a slightly higher open circuit voltage (1.09 V compared to 1.05 V for EVA/MWCNT), which can indicate a better carrier selectivity, while the main difference can be found in the fill factor (FF) values, being 72% for EVA/MWCNT and 69% for EVA/SWCNT. This is mainly caused by a higher series resistance (6.5 $\Omega \cdot cm^2$ for EVA/SWCNT compared to 4.9 $\Omega \cdot cm^2$ for EVA/MWCNT as calculated with a linear fit around the short circuit point), which we attribute to the lower conductivity of the EVA/SWCNT film. Statistics on the performance from the fabrication of a larger number of devices can be found in the supplementary information (**Figure S6**). We emphasize that these devices are not fully optimized and represent a proof of concept, demonstrating that despite the use of an insulating polymer, the EVA/CNT nanohybrids are able to effectively act as charge transport channels, with the insulating polymer not impeding charge transfer from the absorber to the CNT.

CONCLUSION

In summary, we have shown that the inexpensive, insulating EVA polymer is able to bind to and solubilize single- and multi-walled carbon nanotubes, yielding stable and uniform dispersions. By solvent engineering, we are able to remove the excess polymer and thus produce solution-processed films with remarkable conductivity of up to 34 S/cm. These films show good electronic properties and can be employed as selective contacts in perovskite solar cells, delivering a PCE of up to 17.1% and a SPO of 16.1%. Most importantly, this work reevaluates the required properties of the polymer in polymer-functionalized carbon nanotubes for electronic devices, which does not necessarily need to be a conjugated polymer but, remarkably, can be replaced by a simple insulating polymer like EVA.

This process also has a lot of future potential beyond electronic applications, as an inexpensive solubilization of carbon nanotubes in organic solvents can be used for mechanical reinforcement of plastic materials, flame retardant coatings, and other applications where an easy deposition of a well dispersed network of carbon nanotubes can improve the mechanical and electrical properties of materials.

EXPERIMENTAL METHODS

EVA/CNT solution preparation. 5 mg of Ethylene-Vinyl Acetate pellets (ELVAX 150, Dupont, 32% by weight vinyl acetate comonomer content) were dissolved in 10 mL of chlorobenzene (ACROS Organics, ACS reagent grade) by stirring at room temperature for >24h. 5 mg of SWCNTs produced by the HiPCO method[33] (Nanointegris, purified grade) were added to the solution and treated with an ultrasonic probe for 10 min. The mixture was then centrifuged at 10,000 g for 8 min to remove the non-functionalized nanotubes and other impurities. The

supernatant was then collected and added to 20 mL of Toluene (Sigma-Aldrich, puriss. p.a. grade), then heated for 1h to dissolve the excess polymer and induce the aggregation of functionalized tubes. The mixture was then centrifuged at 16,000 g for 4 min and the precipitate, consisting of pellets of functionalized tubes, was collected and dispersed in 10 mL of chloroform (Acros Organic, for HPCL grade, stabilized with 25 ppm amylene). The solution was then treated with an ultrasonic probe for 2 min at ~ 40W output power.

The same procedure is followed for MWCNT/EVA composites, where 1 mg of Nanocyl MWCNTs (Nanocyl, Belgium) nanotubes was used instead of 5 mg of HiPCO tubes.

Conductive film deposition. EVA/CNT films were deposited with a custom-made open science hardware spray coater.[34] Glass substrates (Corning Eagle XG, Thin Film Devices Inc, USA) were sequentially cleaned for 10 minutes in a sonication bath of 2% Hellmanex in de-ionized water, de-ionized water, Acetone, 2-propanol, and treated with a UV-Ozone cleaner for 10 minutes. The samples were attached to the spray coater bed with Kapton tape and kept at 100°C for the whole spraying process. 40 mL of EVA/CNT solution were loaded in a syringe pump and delivered to a nozzle at a rate of 4 mL/min, where a 3 bar compressed air stream atomized the solution. The nozzle was placed at a 45 mm height from the substrates, and it rastered the substrate at a speed of 200 mm/s, covering an area of 62.72 cm^2. The thickness of the film was controlled by diluting the EVA/CNT solution. For an 80 nm thick film, the solution prepared according to the previous section was diluted 3:2 v/v in chloroform for SWCNT and 2:3 v/v for MWCNT.

Solar cell fabrication. 0.05 M tin(IV) chloride pentahydrate (Sigma-Aldrich) was first dissolved in anhydrous isopropanol and stirred for 30 min at room temperature. The solution was deposited on cleaned FTO substrates with 3000 rpm spin rate for 30 s, followed by pre-drying at 100 °C for 10 min and then heat-treated at 180 °C for 1 h. The films were then treated using

chemical bath deposition method: 500 mg urea (Sigma-Aldrich) was dissolved in 40 ml deionized water, followed by the addition of 10 ml 3-mercaptopropionic acid (Sigma-Aldrich) and 0.5 ml hydrochloric acid (37 wt%). Finally, tin(II) chloride dihydrate (Sigma-Aldrich) was dissolved in the solution at 0.002 M and stirred for 2 min. The deposition was made by putting the substrates in a glass Petri dish filled with the above solution, in a 70 °C lab oven for 3 h. The treated substrates were rinsed in a sonication bath of deionized water for 2 min, dried in a stream of nitrogen and annealed for 1 h at 180 °C. 1.45 M perovskite precursor solution was prepared using a 4:1 (v/v) mixed solvent from anhydrous N,N-Dimethylformamide and dimethyl sulfoxide (Sigma-Aldrich) with $FA_{0.83}Cs_{0.17}Pb(I_{0.9}Br_{0.1})_3$ composition using precursor salts: formamidinium iodide (FAI; Dyesol), cesium iodide (CsI; Alfa Aesar), lead iodide (PbI_2 TCI), lead bromide ($PbBr_2$; TCI) and stirred overnight in a glovebox at room temperature. The $FA_{0.83}MA_{0.17}Pb(I_{0.83}Br_{0.17})_3$ was obtained dissolving 1.25 M formamidinium iodide (Dyesol), 0.25 M methylammonium bromide (Dyesol), 0.25 M lead bromide (Alfa Aesar), and 1.375 M lead iodide (TCI) in a 4:1 mixture by volume of N,N-dimethyformamide (DMF) and N,N-dimethyl sulfoxide (DMSO) and stirring it for 15 min at 65 °C. The perovskite precursor solutions were spin-coated through a two-step spin coating program (10 s at 1000 rpm and 35 s at 6000 rpm) with dripping of anisole (Sigma-Aldrich) as anti-solvent during the second step, 10 s before the end. The films were then annealed at 100 °C for 60 min. All films were spin-coated in a drybox with relative humidity below 20%. EVA/CNT solutions have been prepared according to the previous section, diluted 2:3 v/v in chloroform and deposited via spray coating as described. 85 mg of spiro-OMeTAD were dissolved in 1 mL of chlorobenzene by stirring on a hotplate at 90 °C for 10 min. Once cooled down, 33 µL of tert-butylpyridine (tBP) were added, and the solution was deposited by spin-coating at 2,000 rpm for

45 s. Finally, 100 nm thick gold electrodes were deposited by thermal evaporation in a vacuum chamber with base pressure $<7\times10^{-6}$ mbar.

Current−Voltage Measurements. Solar cells performances were measured using a class AAB ABET solar simulator calibrated to give a simulated AM 1.5 spectrum. The intensity of the lamp was calibrated using an NREL-calibrated KG5 filtered silicon reference cell to have an equivalent intensity of 100.0 mW/cm^2 with respect to the measured cell. The current-voltage values were recorded with a Keithley 2400 (Keithley, USA) sourcemeter. The solar cells were masked with a metal aperture defining the active area (0.0919±0.0005 cm^2) of the solar cells, and single-cell contribution was ensured by removing active material between individual cells on the same glass substrate.

Transmittance measurement. All transmittance measurements were carried out using a Perkin-Elmer Lambda 1050 UV-vis-NIR Spectrophotometer using 1 nm steps.

Sheet resistance measurement. Sheet resistance has been measured with a 4 point tungsten carbide probes from Jandel Engineering (0.635 mm spacing) and a Keithley 2450 source meter. A sweep current from -0.2 mA to 0.2 mA (20 points, auto sweep delay, NPLC=1) was applied across the outer probes and the voltage measured across the inner probes, and the sheet resistance was calculated from the slope of the current-voltage curves corrected with $\pi/\ln(2)$ factor for the in-line probe configuration.

PLE maps. Photoluminescence maps were recorded using a custom-made setup. The light source consists of a 75 W xenon lamp focused into a monochromator, and the monochromatic light is split using a 50:50 beam splitter. One beam is recorded by a silicon photodiode and it is used to normalize the excitation intensity, while the other is focused on the sample in a quartz cuvette. The PL from the sample is collected at 90° to the excitation direction and focused onto a spectrograph

fitted with a liquid nitrogen cooled InGaAs photodiode array. Full details of the setup are described elsewhere.[35]

AFM maps. The EVA/CNT solution prepared according to the previous section was diluted 1:5 v/v in chloroform and deposited on a glass substrate by spin coating at 5,000 rpm for 1 minute. AFM images were recorded using an Asylum MFP-3D AFM in non-contact mode, with a scan rate of 0.55 Hz and 512 samples/line.

ASSOCIATED CONTENT

Absorption spectra of EVA/SWCNT and SDBS/SWCNT in solution, Raman spectra of EVA/SWCNT, AFM images of the MWCNT/EVA and SWCNT/EVA films, statistics on the performance of the devices, JV curves of control devices and shelf life sheet resistance measurements of EVA/CNT films are available in the supplementary information. This material is available free of charge via the Internet at http://pubs.acs.org

AUTHOR INFORMATION

Corresponding Authors

* robin.nicholas@physics.ox.ac.uk

Present Addresses

† Chemistry and Nanoscience Center, National Renewable Energy Laboratory, Golden, Colorado 80401, United States (S.N.H.)

Author Contributions

The manuscript was written through contributions of all authors. G.M. conceived and carried out the experiments with help from M.D. for PLE maps, S.N.H. and Z.W. for the solar cells fabrication, M.G.C. for the deposition of the spray-coated films. M.K.R and R.J.N. conceived and supervised the project. All authors discussed the results and have given approval to the final version of the manuscript.

Notes

G.M., M.K.R., R.J.N. are inventors on the UK Patent Application 1719915.9, (date of filing: 30 November 2017) regarding the process described in this work. The authors declare no competing financial interest.

ACKNOWLEDGMENTS

G.M. acknowledges EPSRC for the funding through the Centre for Doctoral Training in New and Sustainable PV (EP/L01551X/1) and University College, Oxford for the Oxford-Radcliffe scholarship. M.K.R. and M.G.C. acknowledge funding from the European Union in FP 7 (Grant No. 630864 and Grant No. 659667 respectively).

REFERENCES

(1) Baughman, R. H.; Zakhidov, A. A.; de Heer, W. A. Carbon Nanotubes--the Route toward Applications. *Science* **2002**, *297* (5582), 787–792.

(2) Bandyopadhyaya, R.; Nativ-Roth, E.; Regev, O.; Yerushalmi-Rozen, R. Stabilization of Individual Carbon Nanotubes in Aqueous Solutions. *Nano Lett.* **2002**, *2* (1), 25–28.

(3) Fong, D.; Adronov, A. Recent Developments in the Selective Dispersion of Single-Walled Carbon Nanotubes Using Conjugated Polymers. *Chem. Sci.* **2017**, *8* (11), 7292–7305.

(4) Bisri, S. Z.; Gao, J.; Derenskyi, V.; Gomulya, W.; Iezhokin, I.; Gordiichuk, P.; Herrmann, A.; Loi, M. A. High Performance Ambipolar Field-Effect Transistor of Random Network Carbon Nanotubes. *Adv. Mater.* **2012**, *24* (46), 6147–6152.

(5) Schießl, S. P.; Fröhlich, N.; Held, M.; Gannott, F.; Schweiger, M.; Forster, M.; Scherf, U.; Zaumseil, J. Polymer-Sorted Semiconducting Carbon Nanotube Networks for High-Performance Ambipolar Field-Effect Transistors. *ACS Appl. Mater. Interfaces* **2015**, *7* (1), 682–689.

(6) Roberts, M. E.; LeMieux, M. C.; Bao, Z. Sorted and Aligned Single-Walled Carbon Nanotube Networks for Transistor-Based Aqueous Chemical Sensors. *ACS Nano* **2009**, *3* (10), 3287–3293.

(7) Cataldo, S.; Salice, P.; Menna, E.; Pignataro, B. Carbon Nanotubes and Organic Solar Cells. *Energy Environ. Sci.* **2012**, *5* (3), 5919–5940.

(8) Habisreutinger, S. N.; Nicholas, R. J.; Snaith, H. J. Carbon Nanotubes in Perovskite Solar Cells. *Adv. Energy Mater.* **2017**, *7* (10), 1601839.

(9) Sprau, C.; Buss, F.; Wagner, M.; Landerer, D.; Koppitz, M.; Schulz, A.; Bahro, D.; Schabel, W.; Scharfer, P.; Colsmann, A. Highly Efficient Polymer Solar Cells Cast from Non-Halogenated Xylene/Anisaldehyde Solution. *Energy Environ. Sci.* **2015**, *8* (9), 2744–2752.

(10) Schuettfort, T.; Snaith, H. J.; Nish, A.; Nicholas, R. J. Synthesis and Spectroscopic Characterization of Solution Processable Highly Ordered Polythiophene–carbon Nanotube Nanohybrid Structures. *Nanotechnology* **2010**, *21* (2), 025201.

(11) Chen, J.; Liu, H.; Weimer, W. A.; Halls, M. D.; Waldeck, D. H.; Walker, G. C. Noncovalent Engineering of Carbon Nanotube Surfaces by Rigid, Functional Conjugated Polymers. *J. Am. Chem. Soc.* **2002**, *124* (31), 9034–9035.

(12) Barber, G. D.; Jorgensen, G. J.; Terwilliger, K.; Glick, S. H.; Pern, J.; McMahon, T. J. New

Barrier Coating Materials for PV Module Backsheets. In *Conference Record of the Twenty-Ninth IEEE Photovoltaic Specialists Conference, 2002.*; IEEE, 2002; pp 1541–1544.

(13) As an indication we report current prices in UK from sigmaaldrich.com: SWCNT 1.3 nm dia: 938 £/g, MWCNT: 105 £/g, rr-P3HT: 419.5 £/g, EVA (vinyl acetate 25 wt%) 0.41: £/g.

(14) Zhang, Z.; Zhai, T.; Lu, X.; Yu, M.; Tong, Y.; Mai, K. Conductive Membranes of EVA Filled with Carbon Black and Carbon Nanotubes for Flexible Energy-Storage Devices. *J. Mater. Chem. A* **2013**, *1* (3), 505–509.

(15) Das, N. C.; Maiti, S. Electromagnetic Interference Shielding of Carbon Nanotube/Ethylene Vinyl Acetate Composites. *J. Mater. Sci.* **2008**, *43* (6), 1920–1925.

(16) Hagen, A.; Hertel, T. Quantitative Analysis of Optical Spectra from Individual Single-Wall Carbon Nanotubes. *Nano Lett.* **2003**, *3* (3), 383–388.

(17) Baskaran, D.; Mays, J. W.; Bratcher, M. S. Noncovalent and Nonspecific Molecular Interactions of Polymers with Multiwalled Carbon Nanotubes. *Chem. Mater.* **2005**, *17* (13), 3389–3397.

(18) Weisman, R. B.; Bachilo, S. M. Dependence of Optical Transition Energies on Structure for Single-Walled Carbon Nanotubes in Aqueous Suspension: An Empirical Kataura Plot. *Nano Lett.* **2003**, *3* (9), 1235–1238.

(19) O'Connell, M. J.; Bachilo, S. M.; Huffman, C.; Moore, V. C.; Strano, M. S.; Haroz, E. H.; Rialon, K. L.; Boul, P.; Noon, W. H.; Kittrell, C.; et al. Band Gap Fluorescence from Individual Single-Walled Carbon Nanotubes. *Science (80-.).* **2002**, *297* (5581), 593–596.

(20) Ado Jorio, Gene Dresselhaus, M. S. D. *Carbon Nanotubes Advanced Topics in the*

Synthesis, Structure, Properties and Applications; 2007; Vol. 111.

(21) Ohno, Y.; Iwasaki, S.; Murakami, Y.; Kishimoto, S.; Maruyama, S.; Mizutani, T. Excitonic Transition Energies in Single-Walled Carbon Nanotubes: Dependence on Environmental Dielectric Constant. *Phys. status solidi* **2007**, *244* (11), 4002–4005.

(22) Stranks, S. D.; Sprafke, J. K.; Anderson, H. L.; Nicholas, R. J. Electronic and Mechanical Modification of Single-Walled Carbon Nanotubes by Binding to Porphyrin Oligomers. *ACS Nano* **2011**, *5* (3), 2307–2315.

(23) Yang, L.; Han, J. Electronic Structure of Deformed Carbon Nanotubes. *Phys. Rev. Lett.* **2000**, *85* (1), 154–157.

(24) Capaz, R. B.; Spataru, C. D.; Tangney, P.; Cohen, M. L.; Louie, S. G. Hydrostatic Pressure Effects on the Structural and Electronic Properties of Carbon Nanotubes. *Phys. status solidi* **2004**, *241* (14), 3352–3359.

(25) Cuddihy, E. F.; Coulbert, C. D.; Liang, R. H.; Gupta, A.; Willis, P.; Baum, B. *Applications of Ethylene Vinyl Acetate as an Encapsulation Material for Terrestrial Photovoltaic Modules*; Pasadena, CA, 1983; Vol. 83.

(26) Naito, M.; Nobusawa, K.; Onouchi, H.; Nakamura, M.; Yasui, K.; Ikeda, A.; Fujiki, M. Stiffness- and Conformation-Dependent Polymer Wrapping onto Single-Walled Carbon Nanotubes. *J. Am. Chem. Soc.* **2008**, *130* (49), 16697–16703.

(27) Sharkey, J. J.; Stranks, S. D.; Huang, J.; Alexander-Webber, J. A.; Nicholas, R. J. Engineering Nanostructures by Binding Single Molecules to Single-Walled Carbon Nanotubes. *ACS Nano* **2014**, *8* (12), 12748–12754.

(28) Habisreutinger, S. N.; Wenger, B.; Snaith, H. J.; Nicholas, R. J. Dopant-Free Planar N–i–p Perovskite Solar Cells with Steady-State Efficiencies Exceeding 18%. *ACS Energy Lett.* **2017**, *2* (3), 622–628.

(29) Jeon, N. J.; Noh, J. H.; Yang, W. S.; Kim, Y. C.; Ryu, S.; Seo, J.; Seok, S. Il. Compositional Engineering of Perovskite Materials for High-Performance Solar Cells. *Nature* **2015**, *517* (7535), 476–480.

(30) McMeekin, D. P.; Sadoughi, G.; Rehman, W.; Eperon, G. E.; Saliba, M.; Horantner, M. T.; Haghighirad, A.; Sakai, N.; Korte, L.; Rech, B.; Johnston, M. B.; Herz, L. M.; Snaith, H. J. A Mixed-Cation Lead Mixed-Halide Perovskite Absorber for Tandem Solar Cells. *Science.* **2016**, *351* (6269), 151–155.

(31) Wang, Z.; McMeekin, D. P.; Sakai, N.; van Reenen, S.; Wojciechowski, K.; Patel, J. B.; Johnston, M. B.; Snaith, H. J. Efficient and Air-Stable Mixed-Cation Lead Mixed-Halide Perovskite Solar Cells with n-Doped Organic Electron Extraction Layers. *Adv. Mater.* **2017**, *29* (5), 1604186.

(32) Wang, Z.; Lin, Q.; Chmiel, F. P.; Sakai, N.; Herz, L. M.; Snaith, H. J. Efficient Ambient-Air-Stable Solar Cells with 2D–3D Heterostructured Butylammonium-Caesium-Formamidinium Lead Halide Perovskites. *Nat. Energy* **2017**, *2* (9), 17135.

(33) Bronikowski, M. J.; Willis, P. A.; Colbert, D. T.; Smith, K. A.; Smalley, R. E. Gas-Phase Production of Carbon Single-Walled Nanotubes from Carbon Monoxide via the HiPco Process: A Parametric Study. *J. Vac. Sci. Technol. A Vacuum, Surfaces, Film.* **2001**, *19* (4), 1800–1805.

(34) AFMD. LANDS - Large Area Nanoparticle Deposition System http://afmd.github.io/LANDS (accessed Jul 5, 2018).

(35) Nish, A.; Hwang, J.-Y.; Doig, J.; Nicholas, R. J. Highly Selective Dispersion of Single-Walled Carbon Nanotubes Using Aromatic Polymers. *Nat. Nanotechnol.* **2007**, *2* (10), 640–646.

Table of Contents/Abstract Graphic: